# Valorization of olive leaf waste as a new source of fractions containing cellulose nanomaterials

Ayman Ben Mabrouk, Jean-Luc Putaux, Sami Boufi

# Valorization of olive leaf waste as a new source of fractions containing cellulose nanomaterials

Ayman Ben Mabrouk[a], Jean-Luc Putaux[b], Sami Boufi[a,*]

[a] University of Sfax - LMSE - Faculty of Science - BP 802 - 3018 Sfax, Tunisia

[b] Univ. Grenoble Alpes, CNRS, CERMAV, F-38000 Grenoble, France

** Corresponding author: e-mail :sami.boufi@fss.rnu.tn - Tel: 216 47274400 - Fax: 21674274437*

Published in: **Industrial Crops & Products** 202 (2023), 116996

DOI: 10.1016/j.indcrop.2023.116996

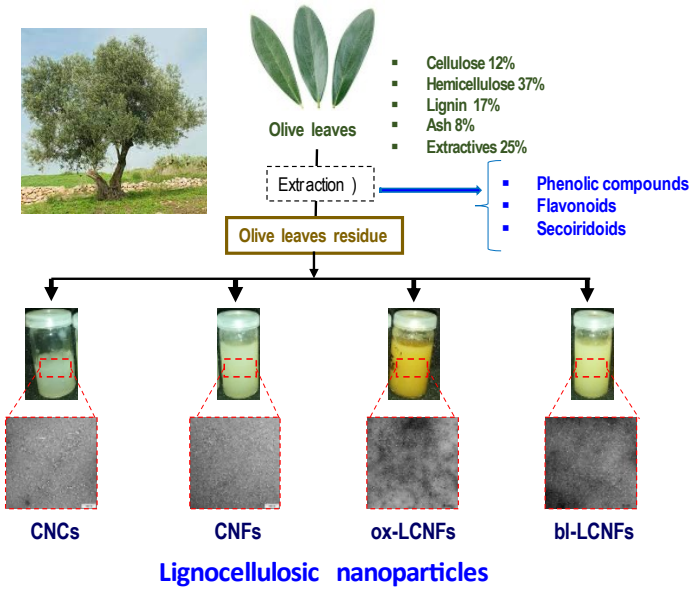



## Abstract

The olive oil activity generates annually a huge amount of biomass waste from the pruning action of the tree and fruit harvesting, including thin woody branches and leaves. In an effort toward more sustainability in the lignocellulosic biorefinery of olive waste activity, nanocelluloses (NCs) were produced from the solid residues remaining after the extraction of biological active compounds from the leaves. Fractions containing cellulose nanocrystals (CNCs), cellulose nanofibrils (CNFs), and lignin-containing cellulose nanofibrils (LCNFs) were prepared and characterized in terms of morphology, chemical composition, thermal stability, colloidal properties, and crystallinity. The reinforcing capability of the different fractions was evaluated in nanocomposite films made of an acrylic matrix incorporating different NC contents. Dynamic mechanical analysis (DMA) and tensile testing of the films were used to compare the reinforcing effect of the NCs. Although CNCs displayed the highest reinforcing effect based on the weight content, LCNFs and CNFs demonstrated also a reinforcing effect, which is higher when normalized with the cellulose content. Compared to CNFs and CNCs, LCNFs displayed a lower hydrophilic character confirmed by contact angle measurement, and had better thermal stability. This work demonstrated the potential use of the solid waste from olive leaves as a new source for biobased nanoparticles containing lignin, hemicellulose components, and cellulose nanofibrils. Beside the high content in bioactive polyphenol compounds that can be extracted from olive leaves, the conversion of the residual biomass can contribute to increasing the circularity and sustainability of olive oil activity.

## 1. Introduction

Switching to lignocellulosic biomass feedstocks as a key resource for the development of biomass-derived material became crucial to reduce the strong dependency on depletable fossil oil resources and for the growth of the bioeconomy based on the valorization of biomass residues. In this sense, fractioning and biorefining the biomass streams are the most promising ways for the upgrading of renewable biomass residues into value products including chemicals, lignocellulosic materials and bioenergy (biofuels and heat) (Chandel et al., 2018; Wang et al., 2020).

Among the different categories of biomass-derived material, nanocelluloses has emerged as one of the most promising and innovative nanostructured materials with broad possibilities of applications in different fields such as composites, coating-additives, cosmetics, paper and board, tissue engineering, packaging, or aerogels. A number of reviews have detailed the applications, production and properties of the different classes of nanocelluloses (Patchiya et al. 2018). Depending on the preparation route, nanocelluloses produced from biomasses can be classified into four categories: cellulose nanocrystals (CNCs), cellulose nanofibrils (CNFs), lignin-containing cellulose nanofibrils (LCNFs) and bacterial cellulose (BNC).

CNFs are flexible nanofibrils with a width typically in the range of 5–50 nm depending on the extent of cell delamination and length in the micron scale (Sujie et al. 2021). They are mainly produced via intensive mechanical shearing to break down the cellulose fibers into their elementary nanofibrils. Lignin-containing cellulose nanofibrils (LCNFs) are a relatively new class of nanocellulose that exhibit the same morphology as CNFs but contains lignin either attached to the fibrils or in the form of nanoparticles (NPs). By its presence, lignin reduces the hydrophilicity of the CNFs and imparts additional properties such as UV-absorption, a better thermal stability, and antioxidant activity (Bian et al 2017, Sadeghifar et al. 2017). CNCs are highly crystalline rodlike particles with an axial elastic modulus in the range of 110–130 GPa (Eichhorn, 2012) and strength around 2–3 GPa, produced by the dissolution of disordered regions of the nanofibrils using chemicals reagents that dissolve or induce chain scission.

With over 65 million olive trees grown on 1.7 million hectares, representing almost 20% of the olive tree orchards worldwide, and an average annual production amounting to $200\times10^3$ tons of produced olive oil, Tunisia is the fourth worldwide producer of olive oil in the world. In addition to olive oil and olives as main products, this production generates different types of lignocellulosic materials such as olive leaves, olive tree pruning, olive stones and pomaces, which generally have no industrial application and are used for animal feed, left or burned in the open air. Therefore, a better utilization of this agricultural residue necessitates its valorization into value-added products and reintroducing them into the economic cycle (Gullón et al. 2018, Sánchez-Gutiérrez et al. 2020).

The stem fraction of olive waste is typically composed of about 40 wt% cellulose, 25 wt% hemicelluloses, 15 wt% lignin, and 20 wt% non-structural compounds including extractives, proteins, and ashes. This woody component can be fractionated via biorefinery processes into various components including cellulose fibers for paper and cardboard (Mutjé et al. 2005), microcrystalline cellulose (Kian et al. 2020), lignin (Santos et al. 2017), energy (Suardi et al. 2020), building materials (Liuzzi et al. 2020), and sugar (Miranda et al. 2019).

The use of stem wastes as a source for the production of nanocelluloses has been reported in several recent works, where CNCs, CNFs and LCNFs were produced, characterized, and tested as additives in a polymer matrix. For instance, CNFs from olive tree pruning were also prepared by TEMPO-mediated oxidation and disintegration by microfluidization (Fillat et al. 2018). Bleached fibers were first prepared by alkali cooking followed by a bleaching treatment. Then, the fibers were oxidized to facilitate disintegration and homogenized at high pressure by microfluidization. CNCs were produced from olive tree pruning wastes through chemical bleaching, and acid hydrolysis ($H_2SO_4$ at 64 % w/v) (Kian at al. 2020). CNCs were shown to inhibit bacterial growth and bacterial biofilm formation, and reduced bacterial epiphytic survival in a comparable way to copper sulfate on leaf surfaces, when used at 1% w/v (Daniele et al. 2022).

LCNFs from olive tree pruning were also produced by TEMPO-mediated oxidation of unbleached alkali-pulps and were included into a PVA matrix up to 7.5 wt% content. The addition of LCNFs contributed to improve the water vapor and oxygen barriers of the film, and imparted a UV-light blocking capacity to the film (Rojo et al. 2015, Sánchez-Gutiérrez et al. 2021).

Olive leaves are another resource of biomass generated from the pruning and harvesting of olive trees, representing more than 20 wt% of the total solid waste from the pruning and harvesting of olives (Romero-García et al. 2014). Thanks to the high content in phenolic bioactive compounds (between 15-120 g/100 g dry leaves), olive leaves were mainly exploited for the extraction of phenolic compounds, which are used in health promoting as cardioprotective, antidiabetic, and anticholesterolemic agents (Talhaoui et al. 2015, Makowska-Wąs et al. 2017), as well as food preservatives (Roselló-Soto et al. 2015). From a circular economy concern and for more sustainable production of the olive oil sector, solid waste from olive leaves extractives can be further valorized into high added value biobased materials.

Considering such advantages, the present work aimed at extracting different types of nanocellulose-containing fractions from olive leaves, including CNCs, CNFs and LCNFs. The resulting nanocelluloses were characterized in terms of morphology, crystallinity, chemical composition, and colloidal properties. In addition, nanocomposite films were prepared by mixing

the nanocellulose suspensions with a waterborne polymer dispersion and the reinforcing effect of the different types of filler was evaluated and compared.

To our knowledge, there is no literature reporting the extraction and characterization of nanocelluloses exclusively from olive leaves. In fact, olive leaves are mainly known as a source of bioactive polyphenols with high added value, that could be extracted using environmentally friendly approaches. However, the amount of olive leaf waste (OLW) recovered after extraction of phenolic compounds is huge (more than 75 wt%) and should be considered as a valuable biomass, in addition to the wood fraction stemming from the annual pruning of the olive tree. OLW can thus be further valorized into high added nanoscale material to further increase the circularity of the olive oil activity.

## 2. Materials and methods

### *2.1. Materials*

Olive leaves (from *Chemlali* variety) were collected in the region of Sfax (center of Tunisia) during May. The solid waste used for the production of NCs was obtained after extraction of the phenolic active compounds using an ethanol/water (1/1 v/v) mixture. The 2,2,6,6-tetramethyl-piperidine-1-oxyl-radical (TEMPO), sodium hydroxide (NaOH), sulfuric acid ($H_2SO_4$) acetic acid ($CH_3COOH$), sodium chlorite ($NaClO_2$), toluene and ethanol were commercial products supplied from Sigma–Aldrich, while bleach was of industrial quality with NaClO content between 4-5% titrated by $Na_2S_2O_3$.

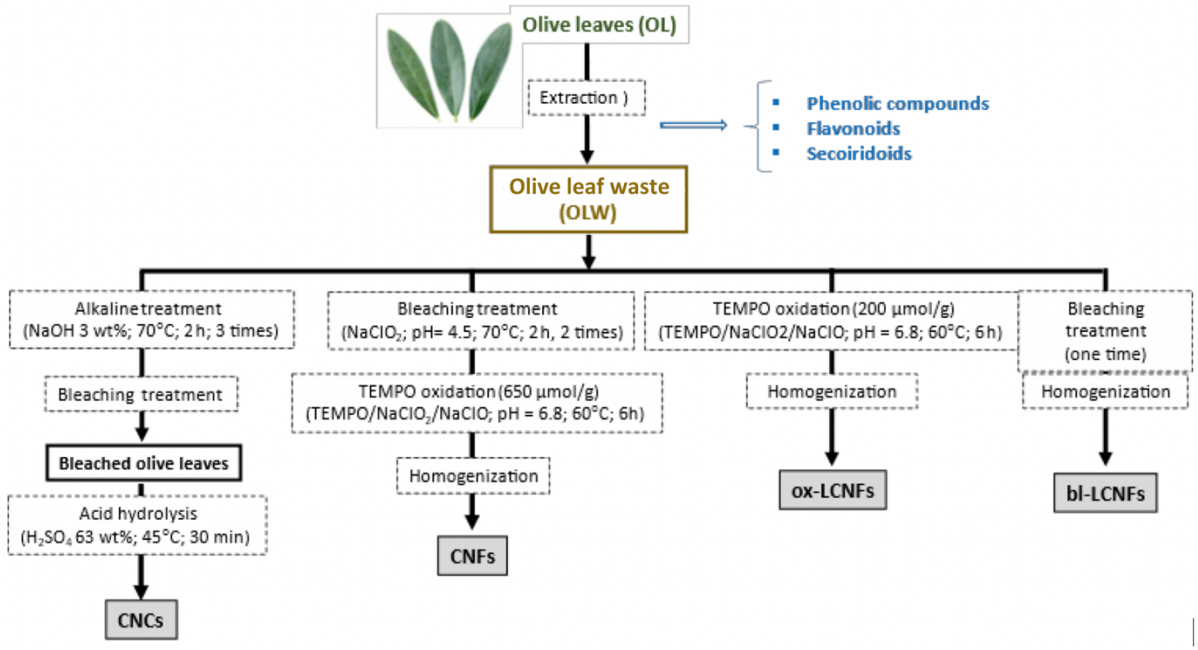


**Figure 1.** Flowchart of the fractionation process of olive leaves detailing the isolation of CNCs, CNFs, bl-LCNFs and ox-LCNFs.

*2.2. Nanocellulose preparation*

The olive leaves were first treated to remove the extractives (mostly phenolic compounds) and the olive leaf waste (OLW) was used as starting material to further extract the nanocellulose fractions. A flow chart of the experimental procedure for the preparation of the CNCs, CNFs, bl-LCNFs and ox-LCNFs is presented in **Figure 1**.

- CNFs: They were prepared from holocellulose extracted from OLW as follows: 10 g of OLW (based on dry weight) was added to 100 g water, 1.5 g of sodium chlorite ($NaClO_2$) and 1.5 mL of acetic acid per gram of OLW were added, and the suspension was kept under mechanical stirring at a temperature of 70 °C for 6 h without the removal of any liquor. Fresh charges of sodium chlorite (0.15 g/g OLW) and acetic acid (0.15 g/g OLW) were added to the reaction every 2 h for up to 6 h. After filtration and washing three times with water, the holocellulose was oxidized under neutral conditions using TEMPO/$NaClO_2$/NaClO system, as follows: 5 g of the holocellulose fibers were dispersed in 200 mL sodium phosphate buffer solution containing $NaClO_2$ (3 g), TEMPO (0.1 g) and bleach with 4 wt% hypochlorite content (20 mL), and the reaction was run at 60 °C for 6 h under magnetic stirring. The carboxyl content of the oxidized holocellulose was around 650 μmol $g^{-1}$. The disintegration of the holocellulose was performed by high-pressure homogenization (HPH) (homogenizer NS1001L PANDA 2 K-GEA, Italy) at a solid content around 2 %, by starting with three passes at 300 bar (4350 Psi) until the suspension turned to a gel, followed by three additional passes at 600 bar (8700 PSI).
- CNCs: OLW was treated twice with 3 wt% NaOH aqueous suspension for 2 h at 70 °C under mechanical stirring. Then, the fibers were bleached using $NaClO_2$/acetic acid at 70 °C for 2 h. The operation was repeated until the cellulose fibers turned white. The fibers were then dried and dispersed in 63 wt % sulfuric acid aqueous suspension at a solid content of around 5 wt%. This suspension was kept at 45 °C under mechanical stirring for 30 min. The suspension was then diluted with water and washed several times by successive centrifugations at 10,000 rpm. A dialysis against distilled water was subsequently performed to remove free acid in the dispersion.
- bl-LCNFs: OLW was submitted to one bleaching treatment. Then, the fibers were disintegrated by HPH following the same procedure as for the CNFs.
- ox-LCNFs: They were prepared by a mild oxidation of OLW (5 g) dispersed in 200 mL water containing $NaClO_2$ (3 g), TEMPO (0.03 g) and bleach (6 mL) and kept under magnetic stirring for 6 h at 60 °C. After washing, the carboxyl content of the nanofibrils was around 200 μmol $g^{-1}$. The ox-LCNFs were submitted to HPH as previously to obtain the ox-LCNF gel.

*2.3. Chemical composition*

The chemical composition of the dried olive leaves was determined after removal of extractives with ethanol/water (1/1) using a Soxhlet. The TAPPI standard method was used for the determination of cellulose (TAPPI T 203cm 1999), Klason lignin (TAPPI T 222 om-83) holocellulose (TAPPI T wd75) and ash (TAPPI T 211 om-93, 2000). The hemicellulose content was calculated by difference of holocellulose and cellulose contents. All tests were performed in triplicates and the average value was reported. It is worth mentioning, that even though the TAPPI method for chemical compositions was defined for wood-based materials, the result obtained for OLW showed a good repeatability, with a difference in composition lower than 10% between the 3 tests.

*2.4. Carboxyl content*

The carboxyl content (CC) of the CNFs and ox-LCNFs was determined by conductometric titration, as elsewhere described (Besbes et al. 2011).

*2.5. Nanosized fraction*

The nanosized fraction (NF) was determined following the methodology reported elsewhere (Besbes et al. 2011).

*2.6. Particle size and ξ- potential measurement*

The particle size and ξ-potential of CNCs, CNFs and LCNFs suspensions were analyzed at 25°C by a particle size and ξ -potential analyzer (Malvern Nano-Zetasizer ZS instrument, UK). The measurements were performed three times for each sample.

*2.7. Transmission electron microscopy (TEM)*

Droplets of dilute nanocellulose aqueous suspensions (0.001 wt %) were deposited onto glow-discharged carbon-coated copper grids and negatively stained with 2 wt % uranyl acetate. All specimens were observed with a JEOL JEM-2100 Plus microscope operating at 200 kV and images were recoded using a Gatan Rio 16 digital camera.

*2.8. X-ray diffraction (XRD)*

Strips of thin films of dried nanocelluloses were fixed on a collimator and X-rayed in transmission and in vacuum with a Philips PW3830 generator (30 kV, 20 mA, CuKα radiation, λ = 0.1542 nm). Two-dimension diffraction patterns were recorded on Fujifilm image plates read with a Fujifilm BAS1800-II bioanalyzer. The 2D patterns were rotationally average to produce XRD profiles.

*2.9. FT-IR analysis*

FT-IR spectra were performed on a Perkin-Elmer Spectrum equipped with a diamond ATR accessory. Five scans were run from 4000 to 600 $cm^{-1}$ wavenumbers.

*2.10. Thermogravimetric analysis*

The thermogravimetric analysis (TGA) of the cellulosic materials was performed on a thermogravimetric analyzer (TGA, PerkinElmer). The dried samples were heated in alumina crucibles from 30 to 800 °C at a rate of 10 °C $min^{-1}$ under air stream.

*2.11. Water contact angle measurements*

Water contact angle (WCA) were measured using a DataPhysics OCA 15 Optical Contact Angle Measuring System (DataPhysics Instruments, Germany). The samples were in the form of thin films prepared by casting.

*2.12. Transmittance measurements*

The optical properties of nanocellulose suspensions and nanocomposite films were assessed by a UV-visible spectrophotometer.

*2.13. Dynamic mechanical analysis*

Dynamic mechanical analysis (DMA) was carried out in tension mode using PYRIS™ Diamond DMA (Perkin-Elmer, Waltham, MA) under heating at 2 °C $min^{-1}$, at a vibration frequency of 1 Hz. The storage (E') and loss (E'') moduli were measured as a function of temperature.

*2.14. Tensile test*

The tensile test analysis was run with a Universal Testing machine (TM2101 V4.23) equipped with a cell load of 500 N. Experiments were performed at room temperature at a rate of 1 and 10 mm $min^{-1}$ for nanocellulose and nanocomposite films, respectively.

## 3. Results and discussion

*3.1. Chemical composition of olive leaves*

The chemical composition of neat olive leaves (OL) (**Figure 2A**) is characterized by a high fraction of extractives (25.5 wt%), which is lower than that reported for Spanish olive leaves (Garcia-Maraver et al. 2013). These extractives are mainly composed of polyphenols compounds including oleuropeosides (oleuropein and verbascoside), flavones, and substituted phenols (tyrosol, hydroxytyrosol, vanillin, vanillic and caffeic acids) (Rodrigues et al. 2015). Beside extractives, OL contained abundant carbohydrates, mainly hemicelluloses (around 37 wt%) and cellulose (12.4 wt%). Lignin and ash were present at 17 and 8 wt%, respectively (**Figure 2A**). The cellulose and lignin contents were close to those reported in the literature for Spanish olive leaves, but the ash, hemicelluloses and extractives contents were different (Lama-Muñoz et al. 2020). Possible reasons for this discrepancy are the time-period of leaf collection and the geographic origin of the olive tree (Markhali et al. 2020). The macromolecular constituents of the leaf cell wall (carbohydrates and

lignin) have a structural function conferring rigidity to the leaf tissue. Their deconstruction into nanoscale components generates biobased particles that might be used as a nanofiller with multiple functionalities.

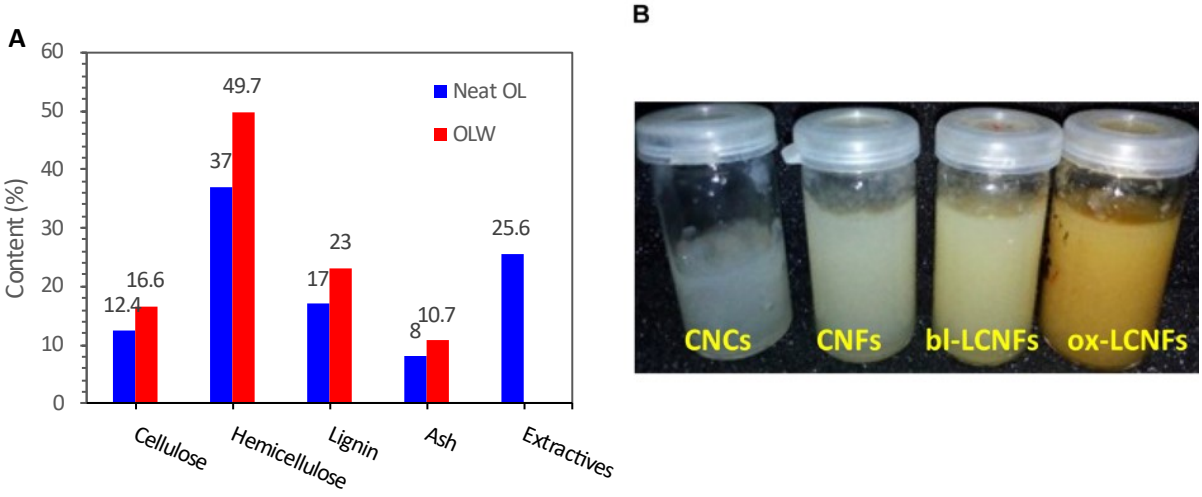


**Figure 2.** (A) Chemical composition of neat OL and OLW after removal of extractive; (B) Photograph of CNC, CNF, bl-LCNF and ox-LCNF suspensions (2 wt% solid content).

*3.2. OLW nanocelluloses*

After the removal of the extractives, the solid residue was submitted to different treatments to destructure the cell walls into lignocellulosic nanomaterials, including LCNFs, CNCs and CNFs, via a chemical route for CNCs, and through high-pressure homogenization for CNFs and LCNFs (**Figure 1**). CNCs and CNFs were prepared from the lignin-free fraction of OL, by conventional acid hydrolysis for CNCs and by HPH of TEMPO-mediated oxidized fibers for CNFs. LCNFs were produced by HPH using either bleached fibers or TEMPO-oxidized crude fibers at a relatively low carboxyl content (around 200 µmol $g^{-1}$). The CNC and CNF suspensions were translucid with a gel-like aspect at a solid content between 1-2 wt%, while the two samples of LCNFs were yellowish with a gel-like aspect at a solid content of 2 wt% (**Figure 2B**).

**Table 1.** Chemical composition and yield of the different samples of NCs isolated from OLW.

| Sample | Cellulose (wt%) | Hemicelluloses (wt%) | Lignin (wt%) | Yield (wt%) |
|---|---|---|---|---|
| CNCs | 96 | 3 | <1 | 14 |
| CNFs | 35 | 64 | <1 | 44 |
| bl-LCNFs | 23.5 | 68 | 8.5 | 76.2 |
| ox-LCNFs | 19.9 | 62 | 18.1 | 60 |

The chemical composition of the different nanocellulose samples and the yield with respect to the solid material after extraction are reported in **Table 1**. As expected, the highest yield was obtained for LCNF samples with a yield exceeding 60 wt%, followed by LCNFs (44 wt%), and the lowest yield was for CNCs (around 14 wt%). The low CNC yield was expected due to the high hemicellulose content and to the method adopted for their preparation which removed the disorganized regions of the nanofibrils. For this reason, the fragmentation of the whole solid residue into nanoscale lignocellulosic material, referred to as LCNFs in the present work, would be more advantageous in terms of sustainability and circularity. In addition, for this later class of nanocellulose, less chemical treatments were involved and less purification steps were necessary, making the conversion of OLW into LCNFs more sustainable and viable from the economic point of view. This also justifies the increasing interest from the scientific community working on nanocellulose in the preparation of LCNFs instead of CNFs.

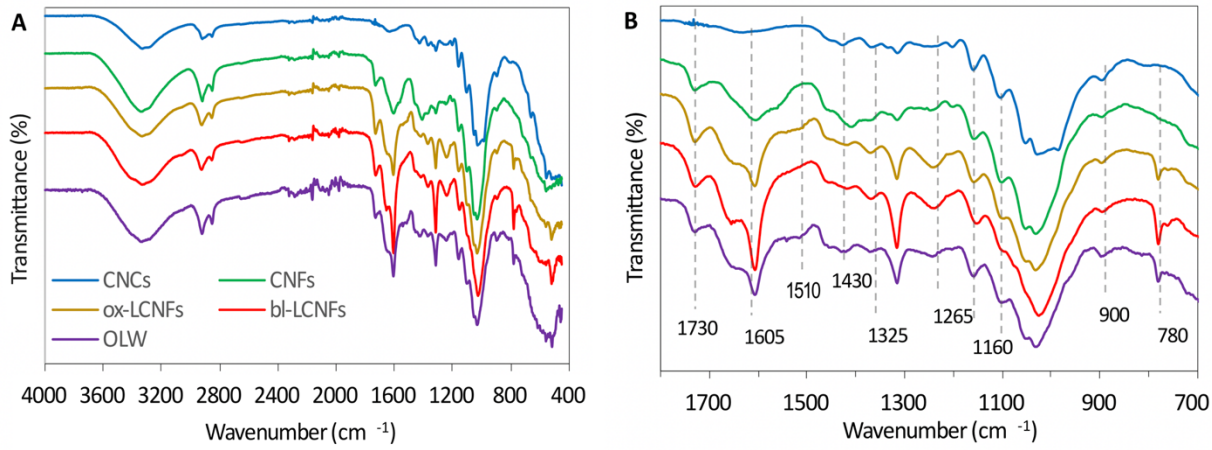


**Figure 3.** FTIR spectra of OLW and the NC samples.

The FTIR spectra of CNCs, CNFs, ox-LCNFs, bl-LCNFs and OLW (after extraction) are shown in **Figure 3**. All samples displayed the characteristic bands of the cellulosic skeleton at 1430, 1160, 1110 and 900 $cm^{-1}$ (Park et al 2010). In the LCNF samples (ox-LCNFs, bl-LCNFs), the characteristic peaks for lignin were visible at 780 $cm^{-1}$ (deformation vibrations of C-H bonds in associated to aromatic rings), 1265 $cm^{-1}$ (C–O stretch of guaiacyl ring), 1325 $cm^{-1}$ (C–O stretch of syringyl ring), 1510 $cm^{-1}$ (aromatic ring vibrations) and 1605 $cm^{-1}$ (aromatic ring vibrations) (Xu et al. 2013, Shi et al. 2019, Pancholi et al. 2022). These bands (except for the one at 1325 $cm^{-1}$) vanished in CNCs and CNFs due to the removal of lignin. The band at 1325 $cm^{-1}$ was still observed with lower intensity for CNFs and CNCs, despite the complete removal of lignin. The emergence of this band is likely due the contribution of C–O–H alcohol groups from cellulose which was reported to give a weak band between at 1315–1330 $cm^{-1}$ associated with the OH

in-plane bending of cellulose (Özgenç et al. 2017). The C=O band at 1730 $cm^{-1}$ observed in OLW, LCNFs and CNFs result from the contribution of acetyl groups and uronic esters of hemicelluloses, and the ester linkage of the carboxylic group of the ferulic acids of lignin (Alemdar and Sain 2008). The intensity of this band decreased in CNFs, due to the removal of lignin and a fraction of hemicelluloses. This band vanished in CNCs due to the complete removal of lignin and hemicelluloses during delignification and hydrolysis.

The size distribution from DLS measurement at pH 6.5-7 is shown in **Figure 4A**. This analysis was run to compare the hydrodynamic volume of the different NC samples. The mean size, corresponding to the maximum in the size distribution plot, was the lowest for CNCs, followed by CNFs, bl-LCNFs, and ox-LCNFs. The smaller size for CNC and CNF suspensions indicates a better individualization of the nanofibrils, while the microscale for LCNF samples may indicate a less efficient fibrillation or a nanofibril aggregation.

The evolution of ζ-potential of ox-LCNF, bl-LCNF, CNC and CNF suspensions as a function of the pH is shown in **Figure 4B.** Both CNCs and CNFs exhibited a high negative ζ-potential around -35 and -45 mV, respectively, which accounts for the high stability of their suspensions for several months. These negative charges result from the presence of the fully ionized sulfate groups and the carboxylic groups, respectively, on the CNC and CNF surfaces. However, the ζ-potential of ox-LCNFs and bl-LCNFs was lower than -20 mV, which was not enough to ensure the stability of the particles and prevent their aggregation at high ionic strength and lower pH (< 4). This lower ζ-potential is explained by the lower CC for ox-LCNFs since the oxidation was mild. For bl-LCNFs, the negative charges originate from the carboxyl groups in hemicelluloses.

The better dispersion and individualization of the CNCs and CNFs were also confirmed from the transmittance measurement through dilute nanocellulose suspensions. As shown in **Figure 4C**, a transmittance above 80 % was reached for CNCs and CNFs, which indicates a high yield of well-dispersed nanosized material. However, for the two LCNF samples, the transmittance was below 30 %, meaning that a high fraction of particles with a width over 200 nm (half of the lowest wavelength of the visible domain) was present and responsible for the decrease in transmittance due to light scattering. The presence of these fractions is supported by DLS measurement, where particles with a size exceeding 2 μm were detected.

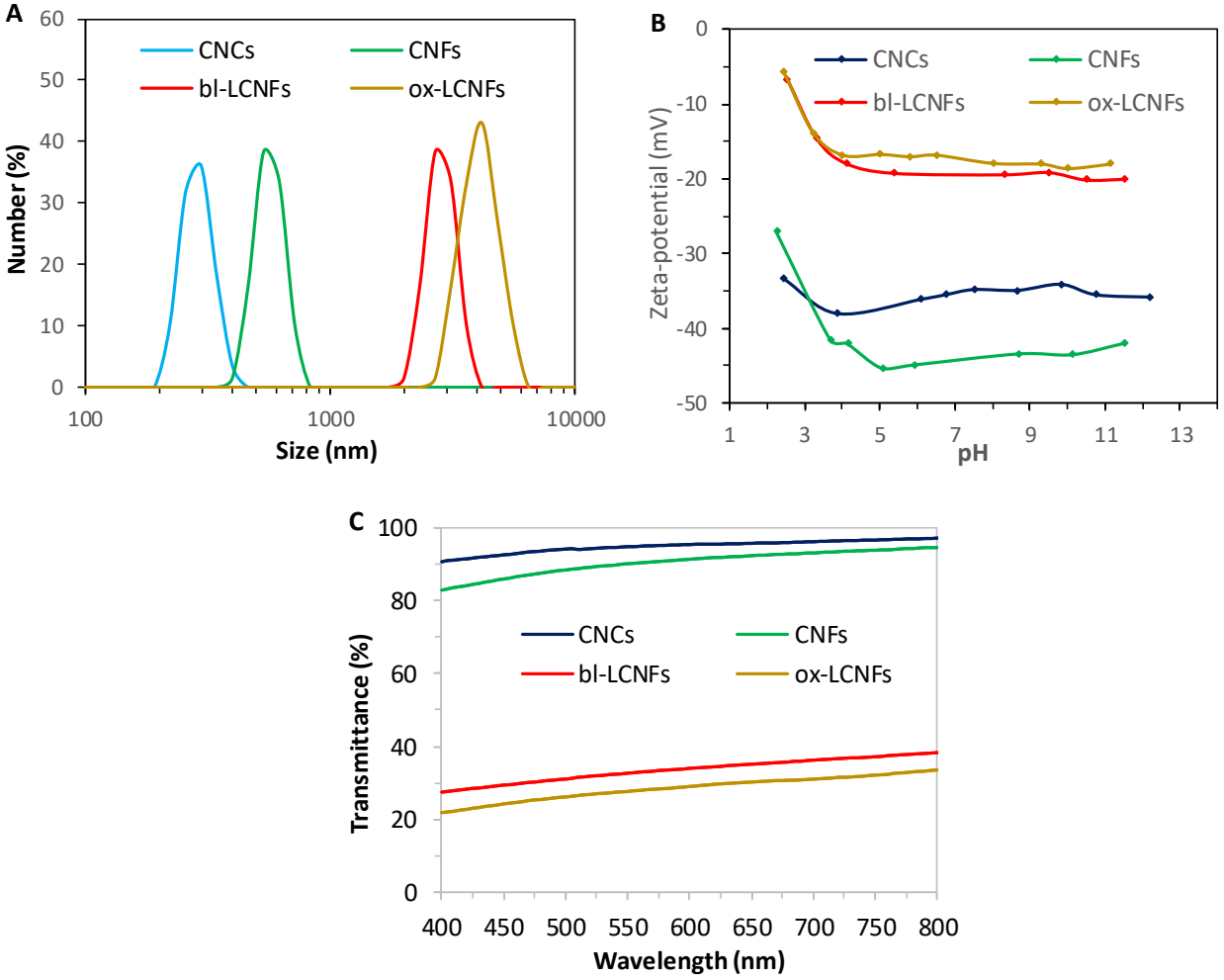


**Figure 4**. (A) Particle size distribution from DLS measurement; (B) $\zeta$-potential as a function of pH; (C) transmittance of CNCs, CNFs, bl-LCNFs and ox-LCNFs in water (0.1 wt%).

CNCs, CNFs, bl-LCNFs, and ox-LCNFs from the supernatants of dilute suspensions were observed by TEM. Both CNCs and CNFs were well dispersed. CNCs were 200-500 nm-long rodlike particles with a width of 3-10 nm, mostly constituted of a few laterally associated elementary units that were not separated upon hydrolysis (**Figure 5A,B**). It is worth mentioning that in comparison with CNCs extracted from woody resources, annual plants or other agricultural waste such as crops, CNCs from OLW are more individual and are longer (Dufresne 2017). CNFs were mostly individual 3-4 nm-wide kinked nanofibrils and bundles of a few fibrils that formed entangled networks (**Figure 5C,D**). bl-LCNFs (**Figures 5E,F**) and ox-LCNFs (**Figures 5G,H**) were also nanofibrillar but many large bundles corresponding to incomplete fibrillation were observed (**Figure S1A,B** and **S1C,D**, respectively). Aside from cellulose nanofibrils, bulkier particle aggregates were present that presumably corresponded to hemicelluloses and/or lignin NPs still present at a high content in these two samples (**Table 1**).

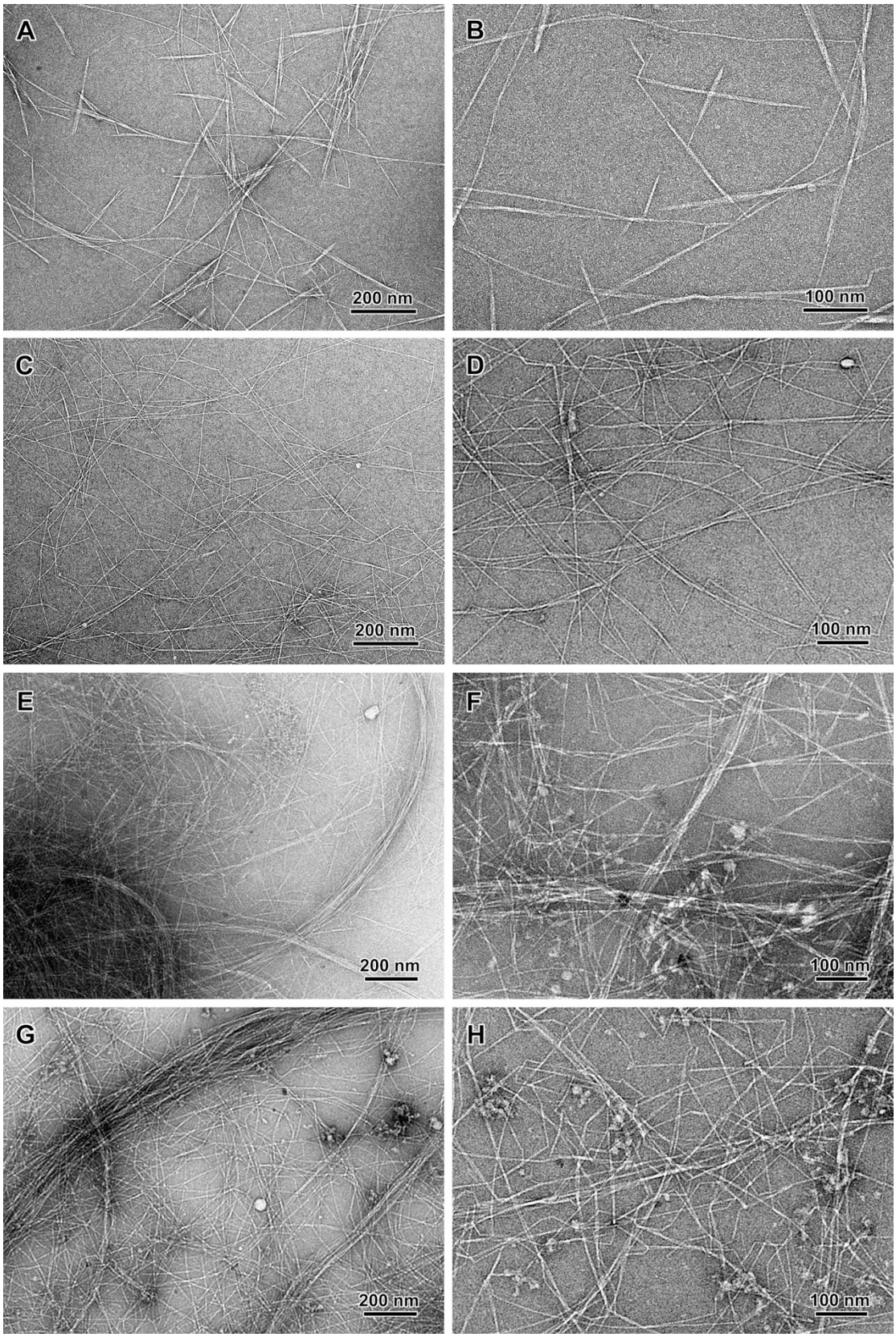


**Figure 5.** TEM images of negatively stained preparations from the supernatants of dilute suspensions of CNCs (A,B), CNFs (C,D), bl-LCNFs (E,F), and ox-LCNFs (G,H).

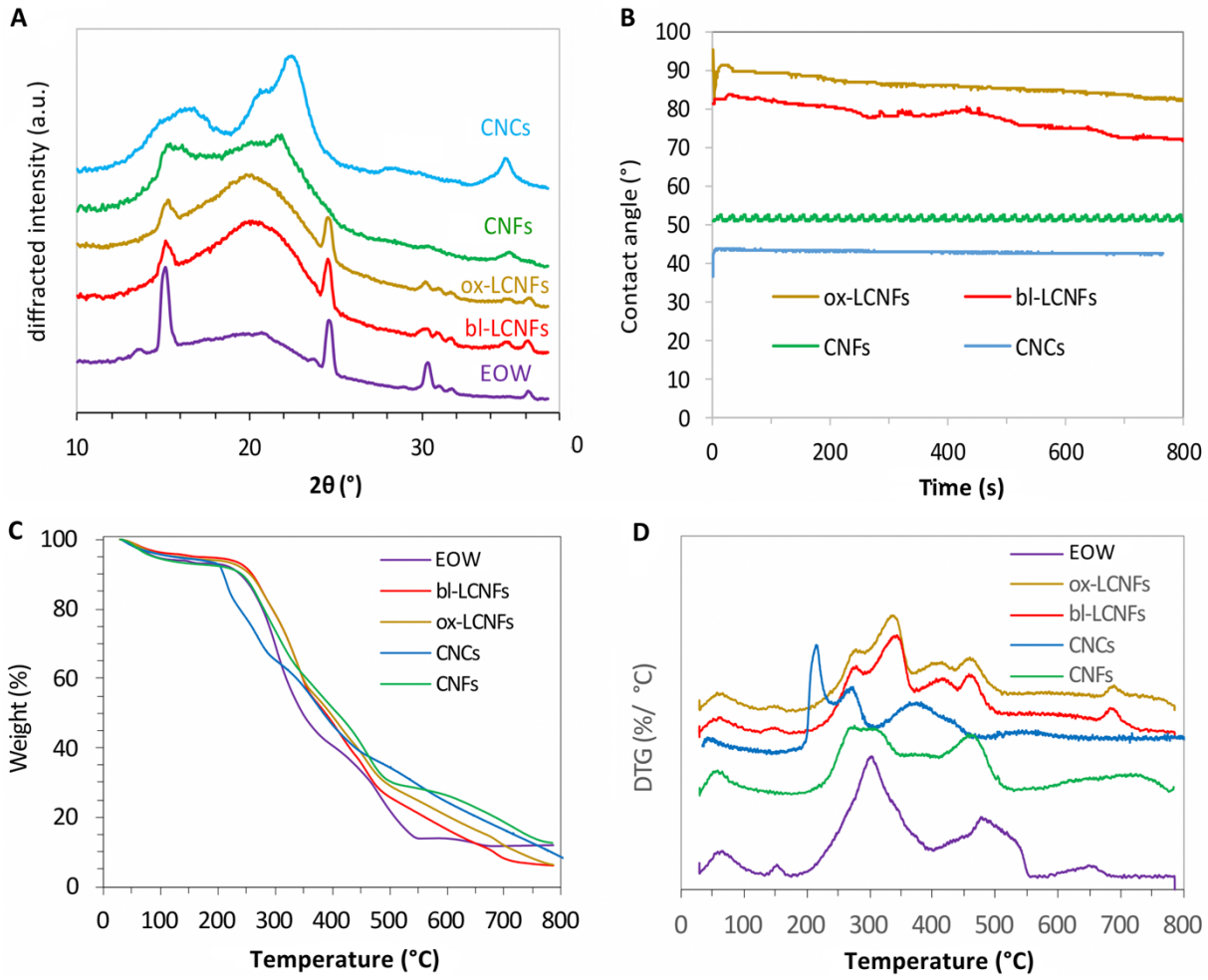


**Figure 6.** (A) X-ray diffraction profiles of OLW and the different NCs, and (B) water contact angle *vs.* time for thin films prepared from the NCs; (C,D) TG and DTG curves of OLW, CNCs, CNFs, bl-LCNFs and ox-LCNFs.

The XRD profiles of OLW and NCs are shown in **Figure 6A**. The narrow diffraction peaks at 2θ = 15.1, 24.8, 30.4, and 36.2° originate from calcium oxalate ($CaO_x$) which is common in drought-resistant plants growing in arid regions. Calcium oxalate has multiple functions essential for plants, especially under stress conditions by providing tolerance against drought, nutrient deprivation, metal toxicity, pathogens, and herbivores. $CaO_x$ is still present but in decreasing relative amounts in ox-LCNFs and bl-LCNFs and is negligible in CNFs. Since CNCs correspond to the cellulose-rich fraction resulting from the extraction of lignin and hemicelluloses from OLW, the XRD profile of the CNC film corresponds to that of native cellulose Iβ, with a broad peak centered at 16.2° corresponding to the overlapping $1\bar{1}0$ and 110 reflections, and two peaks at 22.4 and 34.6° associated with the (200) and (004) crystal planes, respectively (French 2014). Since the disorganized regions of the cellulose nanofibrils were etched away during acid hydrolysis, the CNCs have a high crystallinity degree of 64%. Considering that cellulose is the minor constituent

in OLW, CNFs, ox-LCNFs, and bl-LCNFs (**Table 1**), its contribution to the XRD profiles of these four samples cannot clearly be seen. The influence of lignin and hemicelluloses is thus dominant, yielding a broad peak in the 15-25° region, thus revealing a mostly amorphous character. The contribution at 21.8° observed in the OLW and CNF profiles, and also reported for samples prepared from date palm leaves (Najahi et al. 2023) likely results from the presence of residual epicuticular wax (Khelil et al. 2016). Contributions around 15.8 and 20.3° in the CNF profile could not be ascribed with certainty and may result from the partial recrystallization of a fraction of hemicellulose after the extraction treatment.

The hydrophilic/hydrophobic degree of the different nanocelluloses was assessed by water contact angle measurement on thin film prepared by simple casting and drying at room temperature (**Figure 6B**). The lowest contact angle (CA) was observed for CNCs and CNFs, with a respective CA at 42 and 50°, indicating a hydrophilic surface. This low CA is excepted given the surface chemical composition of CNCs and CNFs dominated by hydroxyl groups, and some ionic/ionizable groups (via $SO_4^-$ and $COO^-$ for CNCs/CNFs respectively). On the other hand, a much higher CA (between 75-85°) was noted for LCNF films, which indicates a material with a relatively lower hydrophilic character than a pure cellulose film. The presence of lignin in LCNFs justifies this higher CA, as lignin is known to impart hydrophobicity, thanks to the presence of the aromatic rings and O-methyl groups.

The thermal stability of the samples was studied by TGA under an air atmosphere, from which the onset of thermal decomposition ($T_{onset}$) was extracted. As shown in **Figure 6C,D**, The least stable nanocellulose was CNCs and CNFs with an onset degradation temperature around 190 and 220 °C, respectively, followed by ox-LCNFs and bl-LCNFs starting to degrade around 245 °C. This difference in the onset of thermal degradation is mainly due to the difference in surface functionality and chemical composition of the nanocellulose samples. Sulfate ($SO_4Na$) and carboxylate (COONa) groups are present on the surface of CNCs and CNFs. Upon heating at about 200 °C, desulfation and decarboxylation occur, which generate an acid-catalyzed reaction that accelerates the degradation (D'Acierno et al. 2020). The absence of these groups in LCNFs and the presence of lignin contributed to enhancing the thermal stability of these NCs, allowing the possibility to mix them with a polymer at a processing temperature higher than 200 °C.

### *3.3. Mechanical properties of nanocomposite films incorporating CNCs, CNFs and LCNFs*

To compare the reinforcing potential of the different nanocellulose samples from OLW, nanocomposite films based on an acrylic matrix were prepared by casting, and the mechanical properties of the films were investigated by DMA and tensile test measurement.

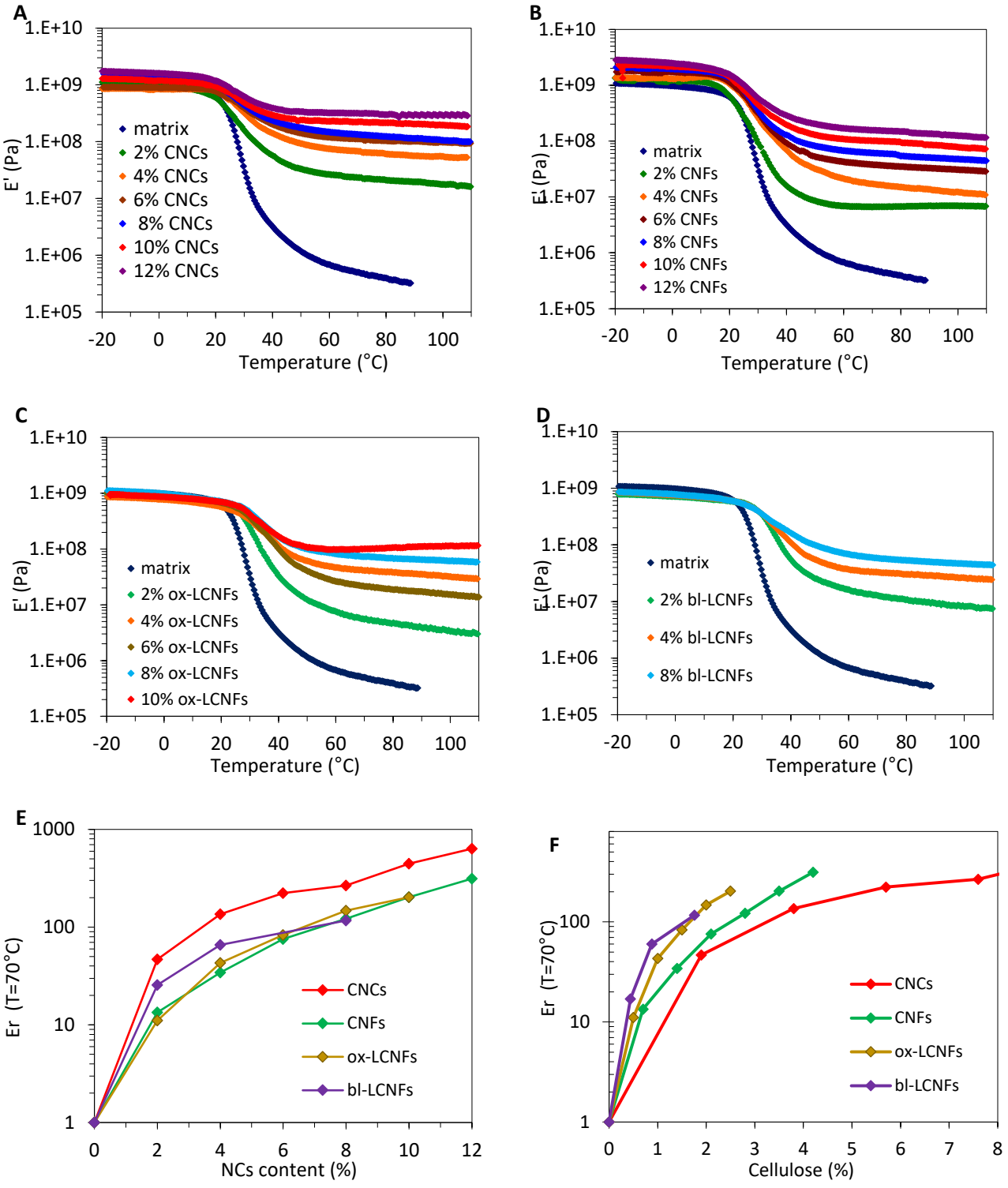


**Figure 7.** (A-D) storage tensile modulus E' vs. temperature at 1 Hz for nanocomposite films based on CNCs, CNFs, ox-LCNFs and bl-LCNFs. (E) evolution of the relative modulus vs CNCs, CNFs, ox-LCNFs and bl-LCNFs content at 70 °C, and (F) the corresponding curves based on cellulose content.

The evolution of the elastic modulus (E′) with temperature for the different composite films incorporating each type of nanocellulose fraction is given in **Figure 7A-D**. For the neat matrix, E′ plot is typical of an amorphous polymer with a transition from the glass to the rubbery domain between 20-30 °C, characterized by a drop in E′ by more than three order of magnitude and a maximum in tan δ at 30 °C. The inclusion of the NCs is accompanied by marked increment in the magnitude of E′, mostly in the rubbery domain, while the effect on the glassy plateau is modest. This effect is expected and in line with the properties of NCs to induce a reinforcing and a stiffening effect when incorporated into a polymer matrix, mainly in the rubbery domain, and provided the NCs were well dispersed within the polymer matrix (Boufi et al. 2014). The reinforcing effect of NCs was ascribed to the set-up of percolated (for CNCs) and entangled networks (for CNFs) among the cellulose NPs held by hydrogen bonding in the interparticle contact regions. This reinforcing effect is affected by several parameters including the aspect ratio, surface functionality, intrinsic modulus, crystalline degree, and flexibility of the of the NCs fibrils. To compare the reinforcing effect of the different NCs, the relative modulus $E_r = \frac{E'_{nan}}{E'_{mat}}$ (with $E'_{nan}$ and $E'_{mat}$ the storage modulus of the composite and unfilled matrix respectively measured in the rubbery region at 70 °C) *vs.* the NC content is presented in **Figure 7E**. For all the NCs samples, $E_r$ markedly increases with the increasing nanofiller content, confirming the strong reinforcing effect of the different classes of NCs from OLW. However, when comparing the reinforcing effect, CNCs demonstrate the most significant stiffening effect. For instance, at 2 and 8 wt% CNC content, $E_r$ was around 46 and 245, while for LCNFs, the increment was around 13 and 115, respectively. This difference in stiffening effect between CNCs and LCNFs may be explained by the difference in the crystalline degree of the NCs, their chemical composition and their morphology. Indeed, the higher crystalline degree of CNCs along with their needle-like morphology, led to a higher intrinsic modulus of the CNCs in comparison with the flexible LCNFs and CNFs as well. However, if we normalize $E_r$ based on the cellulose content of the NCs (**Figure 7F**), a reverse in the stiffening effect can be seen, with the highest effect observed for LCNFs, followed by CNFs and CNCs. This suggests that hemicelluloses and lignin also contributed to the reinforcing effect, albeit their amorphous character. Although less studied than nanocelluloses, several works pointed out an enhancement in the mechanical properties of a composite based on nanolignins (Zhang and Terrasson 2021).

The stress-strain plots for the unfilled matrix and the nanocomposite films with different NC contents are presented in **Figure 8A-D**, from which the tensile modulus (E), and ultimate tensile strength (UTS), were obtained (**Figure 8E-F**). As for DMA analysis, all of the NCs had a beneficial effect on E and UTS for the nanocomposite films, with a magnitude that depended on the type of

NCs. The highest positive effect was noted for CNCs, followed by CNFs, and LCNFs. The huge improvement in E and UTS of the acrylic film with the incorporation of the NCs implies that the films, which could be a coating or an adhesive, became stiffer and with a higher strength compared to the unfilled films. However, the increment in UTS was much lower in the presence of LCNFs in comparison with lignin-free nanocelluloses. This means that at a similar nanofiller content, the aptitude of nanocellulose to enhance the strength of the material decreased when lignin was present. The same reason evoked for the stiffness might also stand for the tensile strength.

The effect of the incorporation of the different nanocelluloses in the films has been studied by transmittance measurement in the UV-Vis domain ranging from 300 to 800 nm at different nanofiller content (**Figure 9A-D**). The spectra have been normalized to a constant thickness (around 200 µm) using the Beer-Lambert law, to avoid any fluctuation due to a difference in film thickness. The neat matrix exhibits a high transmittance (> 80 %) over the visible domain which is indicative of a highly transparent film, thanks to the amorphous character of the acrylic matrix. In the UV-domain, the transmittance decreased to about 70 % due to the presence of styrene in the structure of the acrylic backbone. The incorporation of nanocellulose resulted in a decrease in transmittance, with an effect which depends on the type of nanocellulose. In the presence of CNCs and CNFs (**Figure 9E**), the transmittance levels off to around 52-55 % in the visible domain over a nanocellulose content of 4 wt%, and in the UV-domain, the transmittance exceeded 50 %, indicating a low absorption. That the transmittance remains at an acceptable level (over 50 %) over the whole spectral range is explained, on the one hand, by the nanoscale morphology of the CNCs and CNFs with a width lower than half the wavelength, and, on the other hand, by the good dispersion of the nanofiller within the polymer matrix. This good dispersion is presumably due to the use of the waterborne polymer dispersion that facilitates the processing of the nanocomposite by simple mixing route, without a risk of aggregation of the nanocellulose avoids during film-formation (Dufresne 2017). The low absorption in the UV-domain is due to the absence of lignin in CNCs and CNFs. On the other hand, in the presence of LCNFs (**Figure 9F**), the transmittance decreased with increasing NC content, with a much-marked effect in the UV-domain. This latter effect is due to the presence of residual lignin in LCNFs that strongly absorbs UV light due to the aromatic nature of lignin. The absorption of UV light contributed to protecting the polymer film against photochemical degradation under solar exposition. The steady decline in transmittance with NC content in the visible range indicates a significant light scattering at the nanofiller-matrix interface, that decreases the fraction of transmitted light. The light scattering is due to the presence of NPs with a diameter exceeding 200 nm, presumably resulting from larger bundles of nanofibrils.

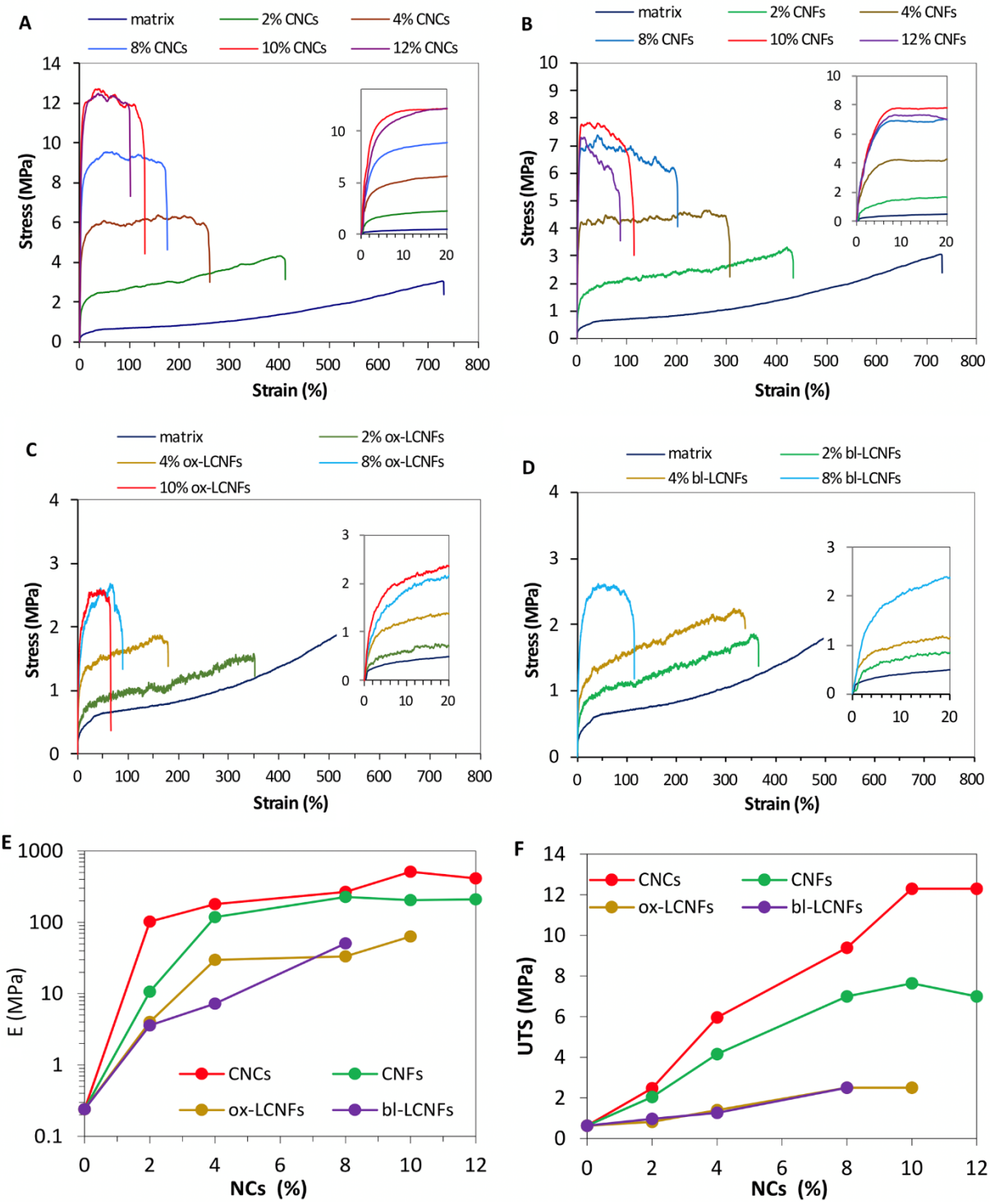


**Figure 8.** (A-D) Stress-strain plots of neat matrix and nanocomposite films incorporating different contents of CNCs, CNFs, ox-LCNFs and bl-LCNFs; (E,F) corresponding tensile modulus (E) and ultimate tensile strength (UTS).

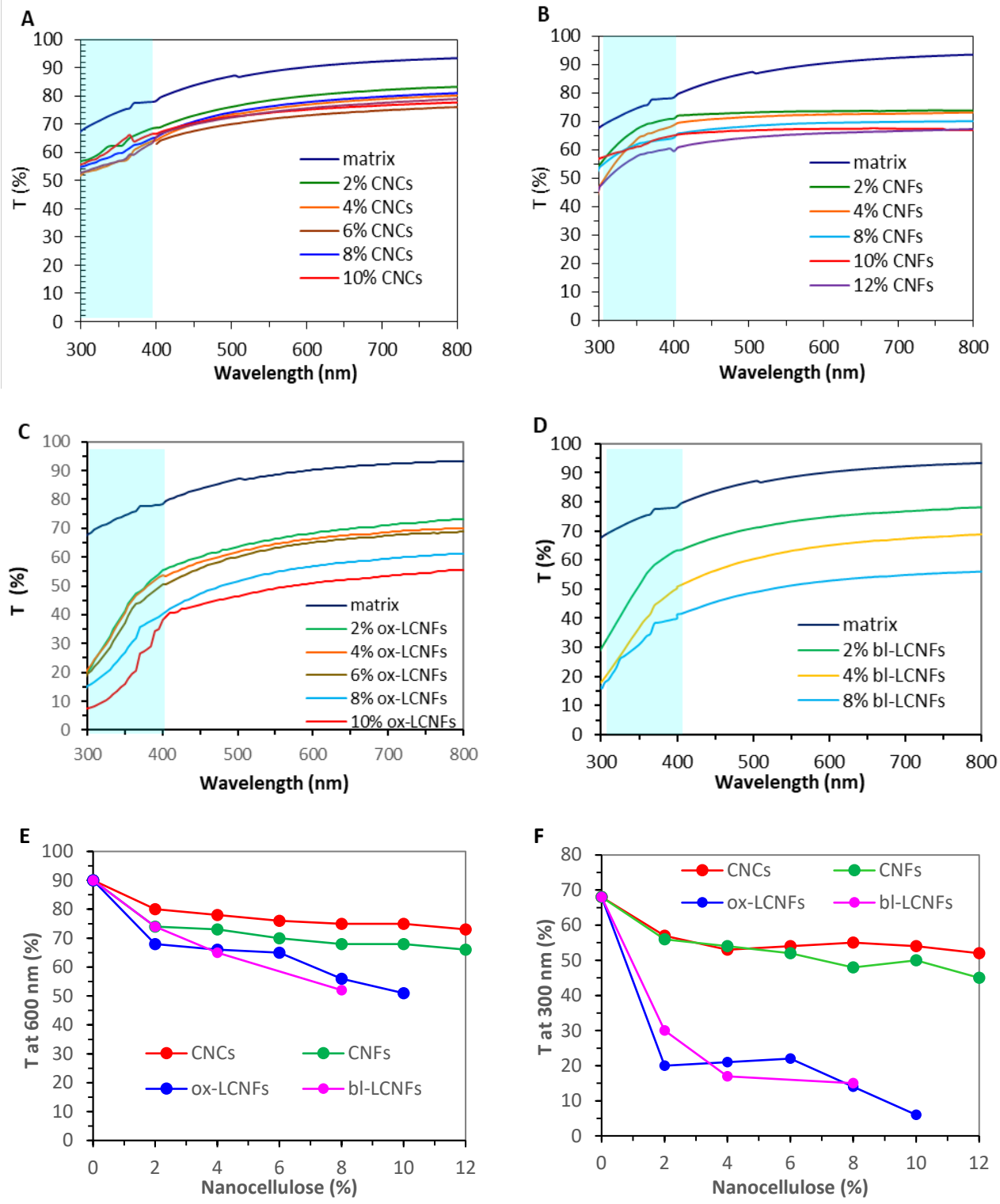


**Figure 9.** UV-Vis transmittance of (A) CNC, (B) CNF, (C) ox-LCNF and (D) bl-LCNF nanocomposite films, (E) Evolution of the transmittance at 600 nm, and (F) at 300 nm for the different films vs. CNC, CNF, ox-LCNF and bl-LCNF content.

## 4. Conclusion

In the present work, the solid waste from extracted olive leaves was used as a feedstock to produce nanocelluloses with different morphologies and chemical compositions. Four nanocellulose grades (CNCs, CNFs and two types of LCNFs) were prepared and characterized. CNCs with a needle-like morphology were prepared by conventional acid hydrolysis, with a yield of around 14 wt%. CNFs with a higher yield of around 44 wt% were prepared from TEMPO-mediated oxidized holocellulose followed by high-pressure homogenization. Both CNCs and CNFs were fairly well individualized with only narrow bundles (width < 10 nm). Two LCNF samples (bl-LCNFs and ox-LCNFs) were produced by high-pressure homogenization of bleached fibers and mildly oxidized neat OLWs. Both types of LCNFs exhibited nearly the same morphology, i.e. long individual or bundled nanofibrils forming entangled networks. Except for highly crystalline CNCs, CNF and LCNF samples were poorly crystalline, which is due to the presence of a high content of hemicelluloses and lignin. On the one hand, the films from pure CNCs and CNFs were hydrophilic, as attested by their water content angle lower than 50°. On the other hand, the LCNF films displayed a lower hydrophilic character with a contact angle exceeding 80°. The lowest thermal stability was observed for CNCs followed by CNFs, with onset thermal degradation ($T_{onset}$) occurring at around 190 and 220 °C, respectively. The LCNFs showed a higher thermal stability, with $T_{onset}$ around 245 °C, presumably due to the presence of lignin. The reinforcing aptitude of the different nanocelluloses was also investigated by casting nanocomposite films. The CNCs had the highest reinforcing effect, followed by CNFs, and LCNFs. The difference was explained by the difference in the crystalline degree of the NCs, their chemical composition, and their morphology. Beside the increase in yield of nanoscale material, the presence of lignin in LCNFs contributed to enhancing thermal stability and imparting a UV-absorption effect that might contribute to enhance the photochemical stability of the nanocomposite films.

The conversion of olive leaves after the extraction of active molecules, into different types of NCs enables the use of residual streams from the olive oil agricultural sector in biorefineries to obtain highly added-valuable biobased products that contribute to the integral valorization of solid wastes from the olive oil agricultural industry by means of a multiproduct cascade biorefinery approach.

**Acknowledgements**

We thank the NanoBio-ICMG Platform (UAR 2607, Grenoble) for granting access to the Electron Microscopy facility. The Ministry of Higher education and Research of Tunisia is acknowledged for financial support through PES 21P2ES-D6P3 Grant.

## References


Alemdar, A, Sain, M., 2008. Isolation and characterization of nanofibers from agricultural residues - Wheat straw and soy hulls. Bioresource Technol. 99, 1664–1671.

Besbes, I., Rei Vilar, M., Boufi, S., 2011. Nanofibrillated cellulose from alfa, eucalyptus and pine fibres: preparation, characteristics and reinforcing potential. Carbohydr. Polym. 86, 1198–1206

Boufi, S., Kaddami, H., Dufresne, A., 2014. Mechanical performance and transparency of nanocellulose reinforced polymer nanocomposites. Macromol. Mater. Eng. 299, 560–568.

Bian, H.Y., Chen L.H., Dai H.Q., Zhu J.Y., 2017. Integrated production of lignin containing cellulose nanocrystals (LCNC) and nanofibrils (LCNF) using an easily recyclable di-carboxylic acid. Carbohydr. Polym. 167, 167–176.

Chandel, A.K., Garlapati V. K., Singh A. K., Antunes F. A. F., da Silva, S.S., 2018. The path forward for lignocellulose biorefineries: bottlenecks, solutions, and perspective on commercialization. Bioresour. Technol. 264, 370–381.

Chen, Y, Fan, D, Han, Y et al. 2018. Effect of high residual lignin on the properties of cellulose nanofibrils/films. Cellulose 25, 6421–6431.

D'Acierno, F., Hamad, W.Y., Michal, C.A., MacLachlan, M.J., 2020. Thermal degradation of cellulose filaments and nanocrystals. Biomacromolecules 21, 3374–3386.

Daniele, S., Sara F., Anna Rita T., Elena F., Giorgio M.B., 2022. Exploring cellulose nanocrystals obtained from olive tree wastes as sustainable crop protection tool against bacterial diseases. Scientific Reports 12, 6149.

Dufresne, A., Nanocellulose: From Nature to High Performance Tailored Materials, De Gruyter GmbH, Berlin/Boston, 2017.

Fillat, Ú., Wicklein, B., Martin-Sampedro, R., Ibarra, D., Ruiz-Hitzky, E., Valencia, C., Sarrión, A., Castro, E., Eugenio, M.E. 2018. Assessing cellulose nanofiber production from olive tree pruning residue. Carbohydr. Polym. 179, 252–261.

French, A.D., 2014, Idealized powder diffraction patterns for cellulose polymorphs. Cellulose 21, 885–896.

García-Maraver, A., Salvachúa, D., Martínez, M. J., Diaz, L.F., Zamorano, M., 2013. Analysis of the relation between the cellulose, hemicellulose and lignin content and the thermal behavior of residual biomass from olive trees. Waste Management 33, 2245–2249.

Gullón, B., Gullón, P., Eibes, G.; Cara, C., De Torres, A., López-Linares, J.C., Ruiz, E., Castro, E., 2018. Valorisation of olive agro-industrial by-products as a source of bioactive compounds. Sci. Total Environ. 645, 533–542.

Khelil, R., Jardé, E., Cabello-Hurtado, F., Khelil, A.O., Esnault, M.-A., 2016. Structure and composition of the wax of the date palm, *Phoenix dactylifera* L., from the septentrional Sahara. Sci. Hortic. 201, 238–246.

Kian, L.K., Saba, N., Jawaida, M., Alothman, O.Y., Fouad, H., 2020. Properties and characteristics of nanocrystalline cellulose isolated from olive fiber. Carbohydr. Polym. 241, 116423.

Kian, L.K., Saba, N., Jawaid, M., Fouad, H., 2020. Characterization of microcrystalline cellulose extracted from olive fiber. Int. J. Biol. Macromol. 156, 347–353.

Lama-Muñoz, A., del Mar Contreras, M., Espínola, F., Moya, Manuel M., Romero, I., Castro, E., 2020. Characterization of the lignocellulosic and sugars composition of different olive leaves cultivars. Food Chem. 329, 127153.

Liuzzi, S., Rubino, C., Martellotta, F., Stefanizzi, P., Casavola, C., Pappalettera, G., 2020. Characterization of biomass-based materials for building applications: The case of straw and olive tree waste. Ind. Crop. Prod., 147, 112229.

Mutjé, P., Pèlach, M.A., Vilaseca, F., García, J.C., Jiménez, L., 2005. A comparative study of the effect of refining on organosolv pulp from olive trimmings and kraft pulp from eucalyptus wood. Bioresource Technol. 96, 1125–1129.

Makowska-Wąs, J., Galanty, A., Gdula-Argasińska, J., Małgorzata, T.-C., Szewczyk, A, Nunes R., Paśko P., 2017. Identification of predominant compounds and cytotoxic activity of olive leaves (*Olea europaea* L. ssp. sylvestris) harvested in south Portugal. Chem. Biodivers. 14, e1600331.

Markhali, F.S., Teixeira, J.A., Rocha, C.M.R., 2020. Olive tree leaves - A source of valuable active compounds. Processes 8, 1177.

Miranda, I., Simões, R., Medeiros, B., Nampoothiri, K.M., Sukumaran, R.K., Rajan, D., Pereira, H., Ferreira-Dias, S., 2019. Valorization of lignocellulosic residues from the olive oil industry by production of lignin, glucose and functional sugars. Bioresource Technol. 292, 121936.

Najahi, A., Tarrés, Q., Mutjé, P., Delgado-Aguilar, M., Putaux, J.-L., Boufi, S., 2023, Lignin-containing cellulose nanofibrils from TEMPO-mediated oxidation of date palm waste: Preparation, characterization and reinforcing potential. Nanomaterials 13, 126. doi:10.3390/nano13010126.

Özgenç, Ö, Durmaz, S, Boyaci, IH, Eksi-Kocak, H. 2017. Determination of chemical changes in heat-treated wood using ATR-FTIR and FT Raman spectrometry. Spectrochimica Acta Part A 171, 395–400.

Pancholi, M.J., Khristi, A., M, A.K., Bagchi, D., 2023. Comparative analysis of lignocellulose agricultural waste and pre-treatment conditions with FTIR and machine learning modeling. BioEnergy Res. 16, 123–137.

Park S., Baker J.O., Himmel M.E., Parilla P.A., Johnson D.K., 2010. Cellulose crystallinity index: measurement techniques and their impact on interpreting cellulase performance, Biotechnol. Biofuel. 3, 10.

Patchiya, P., Prasert, R., Xiaogang, H., Guangwen, X., Abuliti, A., Guoqing, G., 2018. Nanocellulose: Extraction and application. Carbon Res. Conversion 1, 32-43.

Rojo, E., Peresin, M.S., Sampson, W.W., Hoeger, I.C., Vartiainen, J., Laine, J., Rojas, O.J., 2015. Comprehensive elucidation of the effect of residual lignin on the physical, barrier, mechanical and surface properties of nanocellulose films. Green Chem 17, 1853–1866

Romero-García, J.M., Niño, L., Martínez-Patiño, C., Álvarez, C., Castro, E., Negro, M.J., 2014. Biorefinery based on olive biomass. State of the art and future trends Bioresource Technol. 159, 421–432.

Rodrigues, F., Pimentel F.B., Oliveira M.P.P., 2015. Olive by-products: Challenge application in cosmetic industry Ind. Crops Prod. 70, 116–124.

Roselló-Soto, E., Koubaa, M., Moubarik, A., Lopes, R.P., Saraiva, J.A., Boussetta, N., Barba, F.J., 2015. Emerging opportunities for the effective valorization of wastes and by-products generated during olive oil production process: Non-conventional methods for the recovery of high-added value compounds. Trends Food Sci. Technol. 45, 296–310.

Sadeghifar H., Venditti R., Ju, J., Gorga R.E., Pawlak J.J., 2017. Cellulose-lignin biodegradable and flexible UV protection film. ACS Sustain. Chem. Eng. 5, 625–631.

Santos, J.I., Fillat, Ú., Martín-Sampedro, R., Eugenio, M.E., Negro, M.J., Ballesteros, I., Rodríguez, A., Ibarra, D., 2017. Evaluation of lignins from side-streams generated in an olive tree pruning-based biorefinery: Bioethanol production and alkaline pulping. Int. J. Biol. Macromol. 105, 238–251.

Sánchez-Gutiérrez, M., Espinosa, E., Bascón-Villegas, I., Pérez-Rodríguez, F., Carrasco, E., Rodríguez, A., 2020. Production of cellulose nanofibers from olive tree harvest—A residue with wide applications. Agronomy 10, 696.

Shi, Z., Xu, G., Deng, J., Dong, M, Murugadoss, V, Liu, C, Shao, Q., Wu, S., Guo, Z., 2019. Structural characterization of lignin from *D. sinicus* by FTIR and NMR techniques. Green Chem. Lett. Rev. 12, 235–243.

Sujie, Y., Jianzhong, S., Yifei, S., Qianqian, W., Jian, W., Jun, L., 2021. Nanocellulose from various biomass wastes: Its preparation and potential usages towards the high value-added products. Environment. Sci. Ecotechnol. 5, 100077

Suardi, A., Latterini, F., Alfano, V., Palmieri, N., Bergonzoli, S., Pari, L., 2020. Analysis of the work productivity and costs of a stationary chipper applied to the harvesting of olive tree pruning for bio-energy production. Energies 13, 1359.

Sánchez-Gutiérrez, M., Bascón-Villegas, I., Espinosa, E.; Carrasco, E., Pérez-Rodríguez, F., Rodríguez, A. 2021. Cellulose nanofibers from olive tree pruning as food packaging additive of a biodegradable film. Foods 10, 1584.

Talhaoui, N., Taamalli, A., Gómez-Caravaca, A.M., Fernández-Gutiérrez, A., Segura-Carretero, A., 2015. Phenolic compounds in olive leaves: analytical determination, biotic and abiotic influence, and health benefits. Food Res Int 77, 92–108.

TAPPI T 222 om-83, Acid-insoluble lignin in wood and pulp, 1999

TAPPI T 203, Alpha-, beta- and gamma-cellulose in pulp, 1999

TAPPI T 211 om-93, Ash in wood, pulp, paper and paperboard, 2000

TAPPI T wd75, Holocellulose in wood: 1975

Wang, F., Ouyang, D., Zhou, Z., Page, S.J., Liu, D., Zhao, X., 2021. Lignocellulosic biomass as sustainable feedstock and materials for power generation and energy storage. J. Energy Chem. 57, 247–280.

Xu, F., Yu, J., Tesso, T., Dowell, F., Wang, D., 2013. Qualitative and quantitative analysis of lignocellulosic biomass using infrared techniques: a mini-review. Appl. Energy 104, 801–809.

# Supporting information

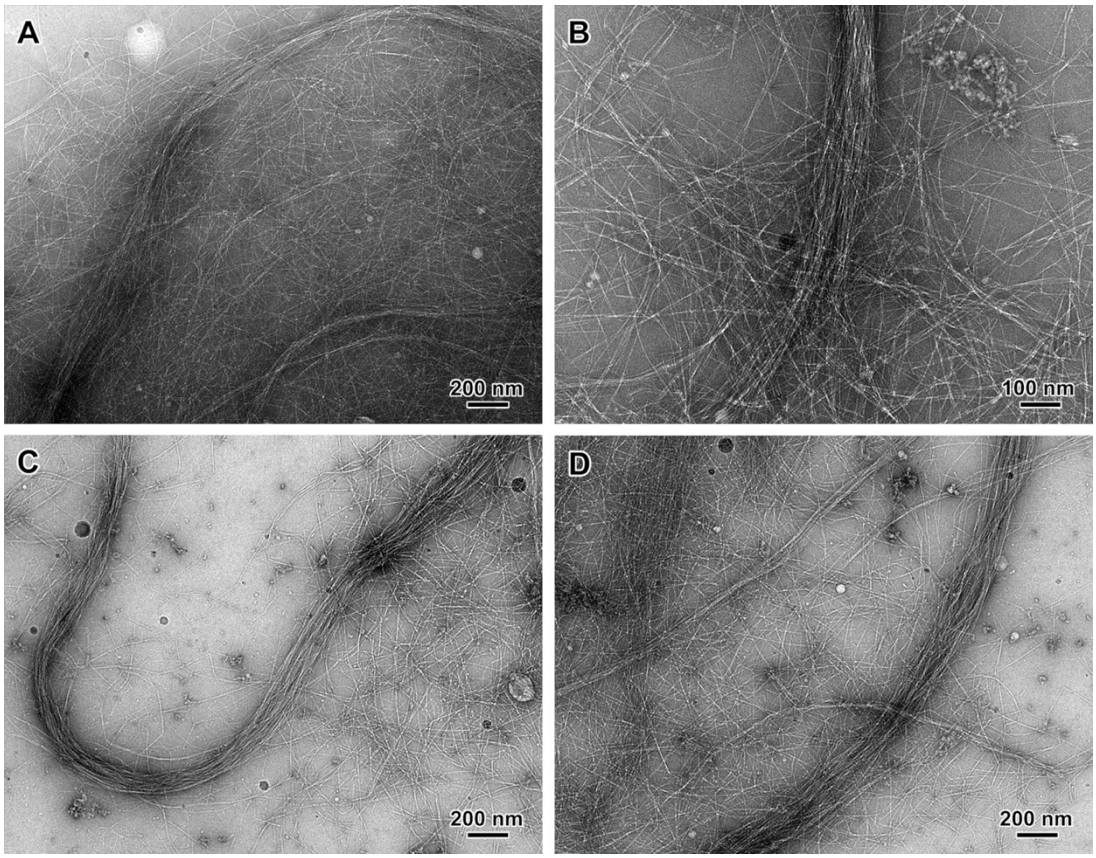


**Figure S1.** TEM images of negatively stained preparations from the supernatants of dilute suspensions of bl-LCNFs (A,B), and ox-LCNFs (C,D).